Improved Approach Based on Meander Line Coil Electromagnetic Acoustic Transducers for A0 Wave Enhancement

LYU Zongmin[1], *GUAN Wei*[2], *ZHANG Yinghong*[1*], *QIAN Zhenghua*[3]

1. School of Mechanical and Electrical Engineering, Guilin University of Electronic Technology, Guilin 541004, P. R. China;
2. State-Owned Chang Hong Machinery Factory, Guilin 541004, P. R. China; 3. College of Aerospace Engineering, Nanjing University of Aeronautics and Astronautics, Nanjing 210016, P. R. China

(Received 1 January 2025; revised 20 May 2025; accepted 27 August 2025)

Abstract: In traditional meander line coil electromagnetic acoustic transducer (MLC-EMAT) structures, the bias magnetic field is usually set to be along the normal direction of plate surface. However, since the particle vibration of the antisymmetric Lamb wave is always dominated by out-of-plane components, using bias magnetic field perpendicular to plate surface is kind of inefficient. In this paper, the performance of both the normal bias magnetic field EMAT (NB-EMAT) and the parallel bias magnetic field EMAT (PB-EMAT) for transmitting and receiving A0 mode Lamb waves are thoroughly studied. The mechanisms of these two structures are elaborated. First, the finite element models of both structures are established. The magnetic fields of these two EMATs are numerically calculated and the results are compared with experiments. Then, the Lorentz force distributions excited by the two EMATs are compared to prove the feasibility of improving the excitation efficiency of MLC-EMAT by selecting the direction of bias magnetic field. Furthermore, the excitation efficiencies of NB-EMAT and PB-EMAT are quantitatively analyzed and compared in simulation software. Results show that the excitation efficiency of PB-EMAT is 108% higher than NB-EMAT. Finally, several groups of comparative experiments are conducted to verify the conclusion obtained through numerical calculation. Experimental results show that by simply replacing the tradition NB-EMAT with PB-EMAT, the excitation efficiency can be greatly increased by more than 50%. If PB-EMATs are used as both the receiver and transmitter, the excitation efficiency can be further increased by 113%.

Key words: electromagnetic acoustic transducer; meander line coil; Lamb wave; A0 wave; parallel bias magnetic field

CLC number: TB552 **Document code:** A **Article ID:** 1005-1120(2025)06-0841-11

0 Introduction

Electromagnetic ultrasonic transducer (EMAT) is one kind of novel devices which directly excites ultrasonic waves in metallic conductors with electromagnetic fields. Compared with piezoelectric transducer, EMAT does not need coupling agent while working and can generate ultrasonic waves in the specimen without direct contact. Besides, using EMAT can selectively excite almost all types of ultrasound, such as Lamb waves, shear-horizontal waves, Rayleigh waves, bulk waves, etc. These advantages make EMAT attractive in the fields of non-destructive evaluation (NDE), non-destructive testing (NDT), and structural health monitoring (SHM) of conductive materials. The earliest studies on EMATs and its further applications on exciting various types of ultrasonic waves were conducted by Thompson and his coworkers[1-4].

Meander line coil EMATs (MLC-EMATs) have been shown to have good directivity. However, the low excitation efficiency of MLC-EMATs makes their engineering application limited[5]. Based

*Corresponding author, E-mail address: yh_zhang@guet.edu.cn.

How to cite this article: LYU Zongmin, GUAN Wei, ZHANG Yinghong, et al. Improved approach based on meander line coil electromagnetic acoustic transducers for A0 wave enhancement[J]. Transactions of Nanjing University of Aeronautics and Astronautics, 2025, 42(6): 841-851.

http://dx.doi.org/10.16356/j.1005-1120.2025.06.010

on simulation and experiment methods, large amounts of researches have been carried out for the optimization of MLC-EMATs, especially the excitation efficiency. Zhang et al.[6] and Du et al.[7] reported their work on optimizing the MLC-EMAT structure and proposed an approach of changing the local bias magnetic field strength using periodic permanent magnets to increase the amplitude of the A0 mode Lamb wave. Liu et al.[8] and Peng et al.[9] demonstrated that in addition to changing the static bias magnetic field, the coil can also be optimized at the same time. The combination of sector-shaped magnet and focused meander-line coils containing uneven split wires not only significantly improves the purity of the A0 wave but also avoids signal distortion. Guo et al.[10] proposed an EMAT consisting of a racetrack coil and a group of periodic permanent magnets (PPMs) that can selectively generate pure symmetric or antisymmetric mode Lamb waves. Pei et al.[11] symmetrically arranged two square magnets with opposite polarities above the meander coil, the local magnetic flux density was then increased, and the excitation efficiency of the MLC-EMAT for surface wave generation and detection was also enhanced. However, the current performance of MLC-EMAT still cannot meet the demands in some specific applications[12-14].

Previous studies were mainly focused on improving the strength of the magnetic field by optimizing the structure of coil or magnet to enhance the output performance. Almost all these studies were conducted based on the assumption that the bias magnetic field is perpendicular to the surface of the plate. Although some scholars have used horizontal bias magnetic field to excite pure A0 mode Lamb wave in their research, these studies are based on periodic magnet structures and cannot explain whether these effects are caused by horizontal bias magnetic field. In recent years, some researchers studied the generation of omnidirectional Lamb waves, and also discussed the influence of different direction of the bias magnetic field[15-16]. It was mentioned in these work that the vertical and horizontal magnetic field should be respectively selected for the excitation of S0 and A0 modes. However, the reasons for this selection were not explained.

It is well known that the displacement of the guided wave in a certain direction is proportional to the corresponding excitation load. Hence, the output performance of EMAT can be enhanced by optimizing the dominant excitation force through adjusting the bias magnetic. This work focuses on studying the influence of bias magnetic field on the excitation efficiency of MLC-EMAT. Firstly, the effect of the bias magnetic field is theoretically analyzed based on the theory of Lorentz force and some qualitatively conclusions are obtained. Furthermore, the magnetic field distribution of a square magnet is calculated and the results are verified by experiment. Finally, the output amplitude of A0 mode Lamb wave excited by both vertical and horizontal bias magnetic field is obtained numerically and experimentally, and the effect of bias magnetic field on the output performance of EMAT is discussed. Through comparative analyses, an optimal magnetic field layout of MLC-EMAT is finally proposed.

1 Fundamental Physics Principle in MLC-EMAT

A typical EMAT consists of a permanent magnet (provides bias magnetic field), a coil on the surface of specimen powered with alternating current, and a specimen. With the design of bias magnetic field and coil structure, various forms of ultrasonic waves can be generated. We only focus on the generation of Lamb wave in this paper. According to the direction of the bias magnetic field, EMATs can be classified into normal biased EMATs (NB-EMATs) and parallel biased EMATs (PB-EMATs). The bias magnetic field of NB-EMAT is perpendicular to the surface of the specimen, while that of PB-EMAT is parallel to the surface of the specimen. Fig.1 shows the configuration of these two types of EMAT, where I is the exciting current, J the eddy current density, L the wire spacing, B the bias magnetic field, and λ the wavelength.

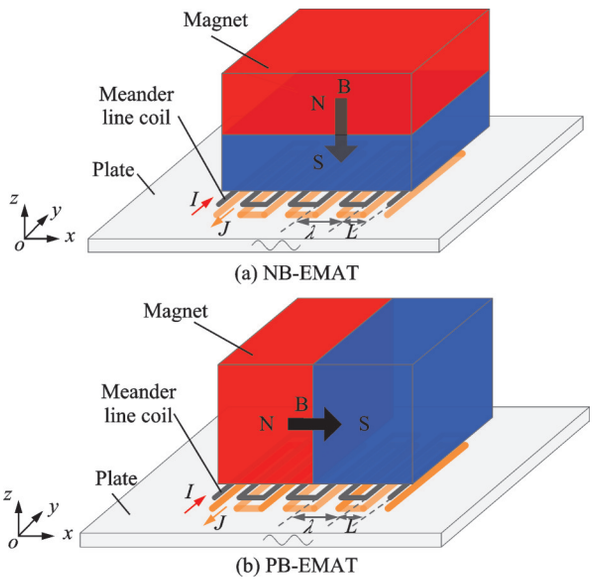

Fig.1 Configurations of the two kinds of MLC-EMAT

1.1 Lorentz force

The operation principle of EMAT is mainly based on the theories of Lorentz force and magnetostriction. When testing a non-ferromagnetic conductive material, only Lorentz force mechanism exists. The basic equation for Lorentz force can be expressed as

$$F = J \times B \tag{1}$$

where F represents the Lorentz force.

When an alternating current flows through the coil, an eddy current arises within the skin depth of the plate. The electrons in the skin depth region vibrate with the deflection of the bias magnetic field, and then generate an alternating Lorentz force. Actuated by this Lorentz force, the material particles in plate will correspondingly vibrate and thereby generate ultrasonic waves.

Expanding Eq.(1) into a scalar form, we have

$$\begin{cases} F_x = J_y \cdot B_z - J_z \cdot B_y \\ F_y = J_z \cdot B_x - J_x \cdot B_z \\ F_z = J_x \cdot B_y - J_y \cdot B_x \end{cases} \tag{2}$$

where F_x, F_y, F_z, J_x, J_y, J_z, B_x, B_y, and B_z are respectively the components of Lorentz forces, eddy currents, and magnetic flux in x-, y-, z-directions. Assume the current in the meander line coil is only in y-direction, i.e. $J_x=J_z=0$, Eq.(2) can be simplified to

$$\begin{cases} F_x = J_y \cdot B_z \\ F_y = 0 \\ F_z = -J_y \cdot B_x \end{cases} \tag{3}$$

It can be seen from Eq.(3) that, when any one of the eddy current density J and the magnetic field strength B is fixed, the magnitude of Lorentz force is proportional to the other. When the excitation current is determined, increasing the magnetic field strength is the only way to increase the amplitude of the ultrasonic wave. This gives an explanation on why previous studies focused on improving the magnetic field strength in the excitation region.

1.2 Lamb wave mode

Under the boundary condition that the upper and lower surfaces of the plate are free surfaces, by means of potential function analysis, the displacement and stress can be obtained as

$$\begin{cases} u_x = [\,\mathrm{i}kA_2\cos(pz) + qB_1\cos(qz)\,] + \\ \qquad [\,\mathrm{i}kA_1\sin(pz) - qB_2\sin(qz)\,] \\ u_z = -[\,pA_2\sin(pz) + \mathrm{i}kB_1\sin(qz)\,] + \\ \qquad [\,pA_1\cos(pz) - \mathrm{i}kB_2\cos(qz)\,] \end{cases} \tag{4}$$

$$\begin{cases} \tau_{zx} = \mu[-2\mathrm{i}kpA_2\sin(pz) + (k^2-q^2)B_1\sin(qz)] + \\ \qquad \mu[\,2\mathrm{i}kpA_1\cos(pz) + (k^2-q^2)B_2\cos(qz)\,] \\ \tau_{zz} = \mu[(k^2-q^2)A_2\cos(pz) - 2\mathrm{i}kqB_1\cos(qz)] + \\ \qquad \mu[(k^2-q^2)A_1\sin(pz) + 2\mathrm{i}kqB_2\sin(qz)\,] \end{cases} \tag{5}$$

where μ is the Lame's constant of material, i the imaginary unit, and k the wave number; A_1, A_2, B_1 and B_2 represent the unknown coefficients of the equation set, respectively; p and q are determined by

$$p^2 = \frac{\omega^2}{c_{\mathrm{L}}^2} - k^2,\quad q^2 = \frac{\omega^2}{c_{\mathrm{T}}^2} - k^2 \tag{6}$$

where ω denotes the angular frequency, and c_{L} and c_{T} are the longitudinal wave velocity and shear wave velocity, respectively.

From Eqs.(4, 5), it is clear that the analytical expressions for displacement and stress are composite functions of sine and cosine containing the variable z, where the sine (and cosine) functions are odd (and even) functions with respect to $x=0$. Thus, the modes propagating in the plate can be classified into two types.

(1) Symmetric mode (S-mode)

$$\begin{cases} u_x = [\,\mathrm{i}kA_2\cos(pz) + qB_1\cos(qz)\,] \\ u_z = -[\,pA_2\sin(pz) + \mathrm{i}kB_1\sin(qz)\,] \end{cases} \tag{7}$$

$$\begin{cases} \tau_{zx} = \mu[-2\mathrm{i}kpA_2\sin(pz) + (k^2-q^2)B_1\sin(qz)] \\ \tau_{zz} = \mu[(k^2-q^2)A_2\cos(pz) - 2\mathrm{i}kqB_1\cos(qz)] \end{cases} \tag{8}$$

(2) Antisymmetric mode (A-mode)

$$\begin{cases} u_x = [\,\mathrm{i}kA_1 \sin(pz) - qB_2 \sin(qz)\,] \\ u_z = [\,A_1 p \cos(pz) - \mathrm{i}kB_2 \cos(qz)\,] \end{cases} \tag{9}$$

$$\begin{cases} \tau_{zx} = \mu[\,2\mathrm{i}kpA_1 \cos(pz) + (k^2 - q^2)B_2 \cos(qz)\,] \\ \tau_{zz} = \mu[\,(k^2 - q^2)A_1 \sin(pz) + 2\mathrm{i}kqB_2 \sin(qz)\,] \end{cases} \tag{10}$$

where the constants A_1, A_2, B_1, B_2 remain unknown. Consider the free boundary condition for the plane strain case with $\tau_{zx}|_{z=\pm h} = 0, \tau_{zz}|_{z=\pm h} = 0$ at $z = \pm h = \pm d/2$. Whereas the displacement, stress and strain fields depend on the structure of the modes, applying the boundary condition yields a system of chi-square equations for A_2, B_1 and A_1, B_2 such that the determinant of the coefficient matrices is zero, giving them non-trivial solutions. Substituting the boundary condition into Eqs.(8,10), we have

$$\frac{(k^2 - q^2)\sin(qh)}{2\mathrm{i}kp\,[\,\sin(ph)\,]} = \frac{-2\mu\mathrm{i}kq[\cos(qh)]}{(\lambda k^2 + \lambda p^2 + 2\mu p^2)\cos(ph)} \tag{11}$$

where λ is the Lame's constant of the material. Using the relationship between wave speed and p, q, and $\lambda = c_{\mathrm{L}}^2 \rho - 2\mu$, and further simplifying, we have the symmetric mode as

$$\frac{\tan(qh)}{\tan(ph)} = -\frac{4k^2 pq}{(p^2 - k^2)^2} \tag{12}$$

And the antisymmetric mode as

$$\frac{\tan(qh)}{\tan(ph)} = -\frac{(q^2 - k^2)^2}{4k^2 pq} \tag{13}$$

Eqs.(12, 13) are the well known Rayleigh-Lamb frequency equations. These equations can be used to determine the phase velocity corresponding to the thickness product of a wave propagating in a plate at a certain frequency.

For Lamb wave mode, the in-plane displacement and out-of-plane displacement are proportional to their corresponding excitation force F_x and F_z, respectively[17-18]. In order to further illustrate the relationship between Lorentz force and displacement, we applied vertical and horizontal load to the aluminium plate to simulate the vertical and horizontal Lorentz force in the plate, respectively. Figs.2(a, b) show the propagation of Lamb waves in the plate under vertical and horizontal loading, and it can be seen that the amplitude of the A0 wave is larger than that of the S0 wave in both cases, but the amplitude of the S0 wave for the horizontal load is larger with respect to that of the S0 wave for the vertical load. Figs.2(c,d) show the displacement amplitude of in-plane displacement u and out-of-plane displacement v in the plate under vertical and horizontal loading, respectively. By comparison, it can be found that the A0 wave amplitude of the out-of-plane displacement v is larger than the in-plane displacement u under vertical loading, while the S0 wave amplitude of the in-plane displacement u is larger than the out-of-plane displacement v under horizontal loading. The in-plane displacement mainly correspond to the resulting S0 wave and the out-of-plane displacement mainly correspond to the resulting A0 wave.

It is worth noting that, as shown in Fig.2, the S0 wave propagates faster than the A0 wave. How-

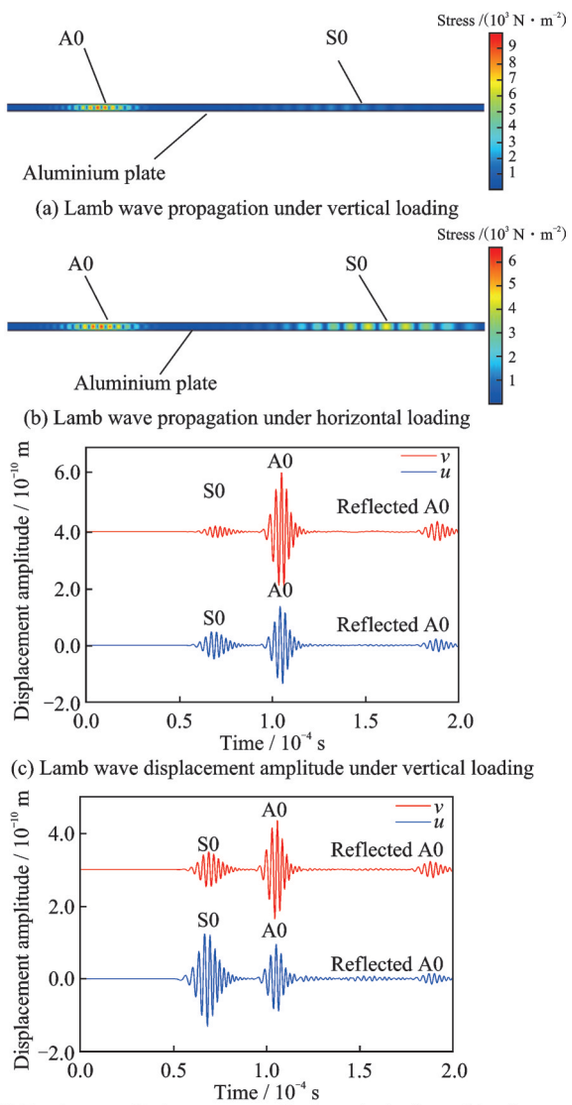

Fig.2 Lamb wave modes under vertical and horizontal loadings

ever, the S0 wave is not observed in the reflected wave. This is because the S0 wave experiences greater attenuation during propagation and reflection, and the amplitude of the excited S0 wave is inherently smaller than that of the A0 wave. As a result, the reflected S0 wave is nearly obscured by noise.

Therefore, to maximize the output amplitude of A0 mode, we should make F_z as large as possible and F_x as small as possible so as to attenuate the interference of S0 mode wave. Then, one needs to carefully design the configuration of EMAT to achieve maximum F_z is particularly important. In next section, the arrangement of magnet will be studied and an optimal configuration which can excite maximum F_z will be proposed.

2 Analysis of Bias Magnetic Field and Distributions of Lorentz Force

In this section, the bias magnetic field provided by a permanent magnet is simulated first, and the simulation result is compared with the experimental one. Then distributions of Lorentz force excited by normal and parallel bias magnetic field are also simulated. The excitation efficiencies of these two types of EMATs (NB-EMAT and PB-EMAT) are quantitatively evaluated through comparison.

In order to correctly simulate the distributions of Lorentz force, we need to obtain some necessary parameters of the working point. The dispersion characteristic curve of Lamb wave in the aluminium plate of non-ferromagnetic material is shown in Fig.3. With increasing the frequency-thickness product, multiple modes appear in the Lamb wave. Therefore, the selected operating point should be as small as possible to reduce the modes of the Lamb wave. The working point chosen for this study is shown in Fig.3. The frequency-thickness product is 1 100 kHz·mm. The phase and group velocities of the A0 and S0 modes are 2 387 m/s and 5 285 m/s, 3 148 m/s and 5 036 m/s, respectively. The thickness of the aluminium plate used is 3 mm. Therefore, it can be determined that the excitation frequency f of the MLC-EMAT in this paper is

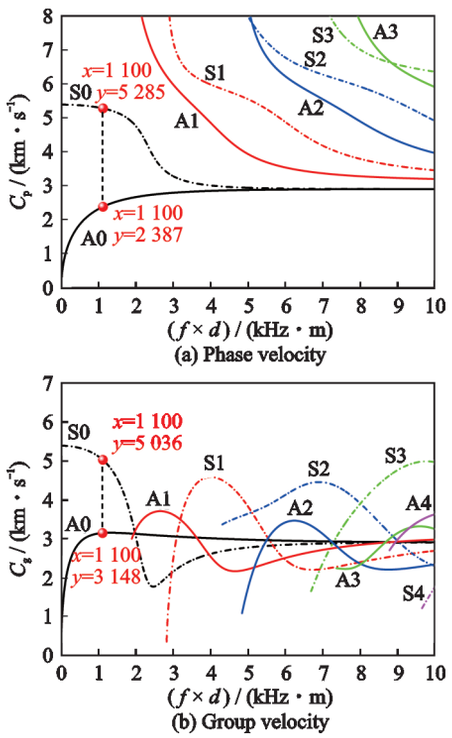

Fig.3 Lamb wave dispersion characteristic curves of aluminium plate of non-ferromagnetic material

367 kHz and the wavelength λ of A0 wave is 6.5 mm.

The EMAT models are set up in well-developed finite element software COMSOL multiphysics. For the analyses in this paper, the coupling between electromagnetic field and mechanical field needs to be considered. The "AC/DC, Magnetic Fields" module (provided in the software) is added, and the "Ampère's Law" and "Coil" interfaces are used to create static bias magnetic field and induce eddy current in the plate. The bias magnetic field is provided by a cubic magnet with a side length of 30 mm, and the residual magnetic flux density of this magnet is 1.2 T. The lift-off of the magnet is 2 mm. The coil is made of square-section copper wire with the width of 1 mm, the thickness of 0.5 mm, and 10 turns to ensure sufficient eddy current density. The aluminium plate is made of 7 075 aerospace aluminium alloy, with material properties shown in Table 1. In the model, the aluminium plate has the diameter of 1 000 mm and the thickness of 3 mm. The Lorentz force is determined by the bias magnetic field and eddy current density, and is calculated using the "Body Load" interface in

Table 1 Performance parameters of 7075 aerospace aluminium alloy material

Material designation	Tensile strength/MPa	Electrical conductivity/(10^7 S•m^{-1})	Elastic modulus/GPa	Poisson's ratio	Density/(g•cm^{-3})
7075	524	3.774	71	0.33	2.81

the "Solid Mechanics (Elastic Waves)" module. The balance between fine mesh and computational storage resources in simulation studies plays a decisive role in the accuracy of the solution results. A triangular mesh was selected in this study due to its better robustness. To maintain both accuracy and computational efficiency, the mesh size for critical components (coils, magnet, and aluminium plate) was set to 1/10 of the wavelength. And eight boundary layers were set on the surface of the aluminium plate, while the remaining mesh was divided using a regular grid. An observation line (Line 1) is set under the magnet from $x=-25$ mm to $x=25$ mm for the discussion and comparison of calculated results.

2.1 Analysis of bias magnetic field

The spatial distributions of static magnetic flux density are shown in Fig.4. For quantitative comparison, we experimentally measure the magnetic field distribution of a real magnet with a nominal magnetization of 1.2 T. The size of the experimental magnet model is the same as the finite element model. A Tesla meter with a Hall sensor probe is used to measure the magnitude of magnetic field. The measuring positions are set on the observation line as defined in the simulation model, and the measured data is collected every 0.5 mm. After measurement, we obtained the B_x and B_z values corresponding to several points. By using data fitting, we can get the B_x and B_z curves corresponding to the actual magnet. Results of the magnetic field distribution on the observation line obtained by simulation and experiment are both shown in Fig.5.

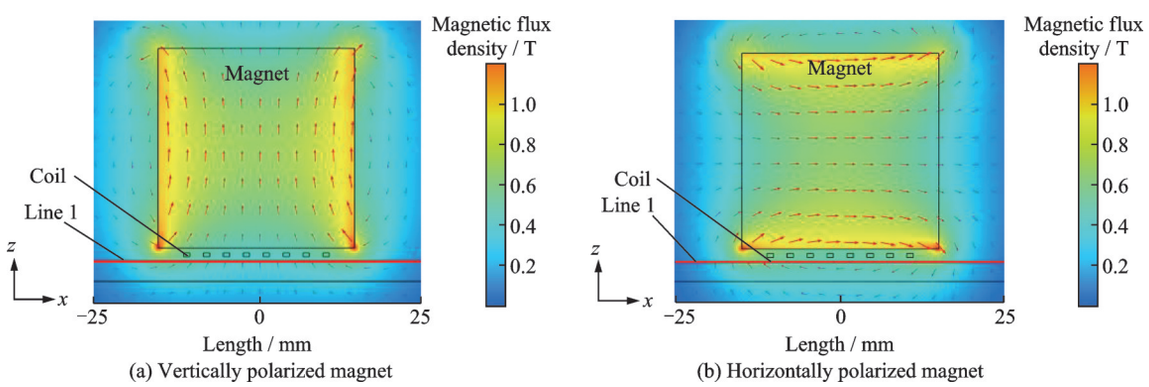

Fig.4 Spatial distribution of static magnetic flux density

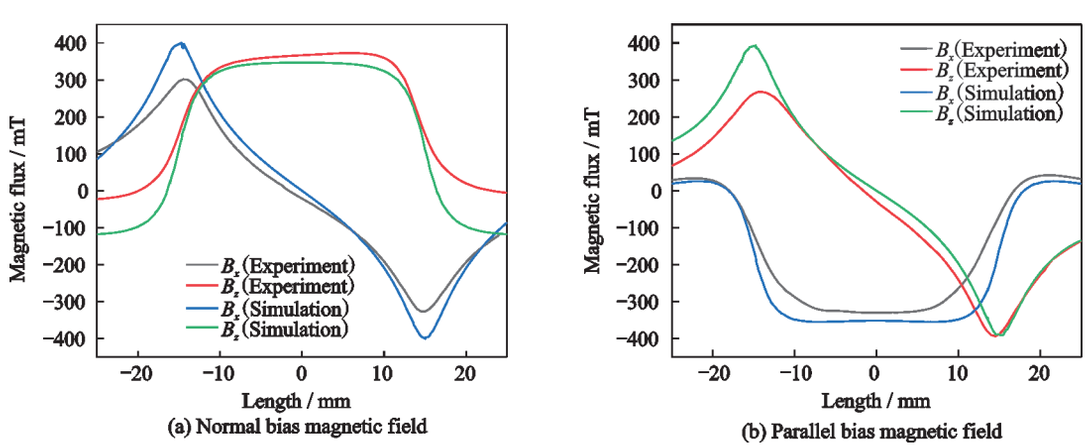

Fig.5 Distribution of static magnetic flux density on the observation line

From the comparison, the accuracy of simulation results and the experimental results can be verified. Fig.5(a) shows the magnetic field distribution on the observation line when the magnet is vertically polarized. The experimentally measured B_x is smaller than the simulated value, while the experimentally measured B_z is larger than the simulated value. Besides, the experimentally measured distribution line of B_z is obviously asymmetric along x-direction, with a larger value on the right half side. Fig.5(b) shows the magnetic field distribution on the observation line when the magnet is horizontally polarized. The maximum amplitude of experimentally measured B_x and B_z are smaller than the simulated one. The inconsistencies of the magnetic field distribution mentioned above are mainly induced by uneven polarization in real magnet.

2.2 Analysis of Lorentz forces

A modulated five-peak sinusoidal current is fed into the coil with an amplitude of 20 A and a frequency of 367 kHz. The time step of transient solution is set to be 1/20 of a signal period. The local transient distribution of the Lorentz force density F in the plate is shown in Fig.6. The size and direction of the red arrow respectively indicate the magnitude and direction of the Lorentz force. From Fig.6(a) we can find that the Lorentz force generated by NB-EMAT is dominated by its horizontal component, especially in the central area where the magnetic direction is almost vertical to the plate surface. As for the Lorentz force generated by PB-EMAT, shown in Fig.6(b), the out-of-plane component is dominant.

The transient distributions of the Lorentz force on the observation lines (defined in Fig.4) are shown in Fig.7. The curve shapes of the Lorentz force components F_x and F_z generated by NB-EMAT and PB-EMAT are nearly opposite, which is because the magnetic field of the normal bias magnet is opposite to that of the parallel bias magnet. It is worth noting that the amplitude of F_z induced by PB-EMAT is 64% larger than F_x induced by NB-EMAT although their curve shapes are similar, which means that the excitation efficiency of PB-EMAT to exciting out-of-plane displacement is higher than that of NB-EMAT.

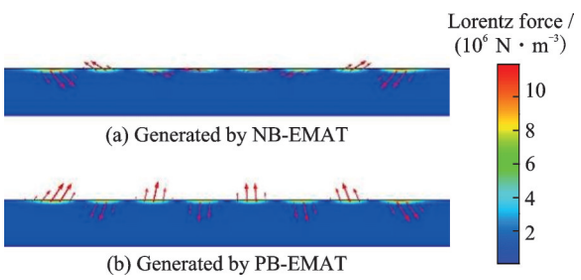

Fig.6 Transient distribution of Lorentz force density in aluminum plate

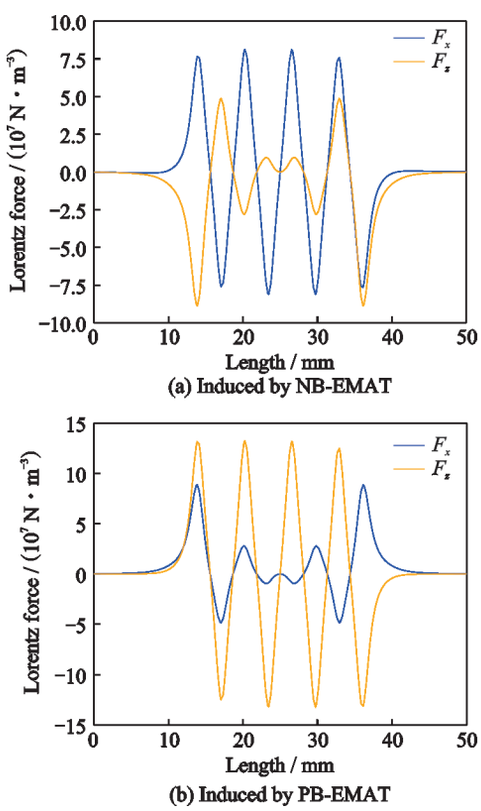

Fig.7 Calculation results of the distribution of induced Lorentz force

We compared and analyzed the magnetic field and Lorentz force generated by the two EMATs. According to Eq.(3), when the excitation current remains unchanged, increasing B_x increases the corresponding F_z, which contributes to the corresponding A0 wave. The simulation results of the PB-EMAT are in complete agreement with the theoretical analysis. Therefore we can conclude that PB-EMAT is more suitable for exciting A0 mode Lamb waves.

3 Influence of Bias Magnetic Field on Guided Wave Mode

3.1 Finite element analysis

Generally, the spacing L of the meander line coil approximately equals to the half-wavelength $\lambda/2$ of the guided wave. In the following descriptions, one coil wire is defined as a "channel". For the generation of A0 mode in EMAT model, to make the magnet cover the coil completely, the number of channel is taken to be 8. The measuring point is 250 mm away from the EMAT. Fig.8 shows the excited displacement amplitude under different bias magnetic fields. The propagation speed of the first wave packet and second wave packet are 5 051 m/s and 3 246 m/s, respectively. Their propagation velocities are all close to the theoretical group velocities of the S0 mode and A0 mode Lamb waves at the excitation frequency of 367 kHz. The relative errors are only 0.3% and 3.1%. Therefore, it can be determined that the first wave packet of PB-EMAT in Fig.8 is the S0 wave and the second wave packet is the A0 wave. Through comparison, we can find that the amplitude of A0 mode excited by PB-EMAT is 108% larger than that excited by NB-EMAT. The simulation results also indicate that the out-of-plane displacement amplitude is positively related to the magnitude of out-of-plane Lorentz force.

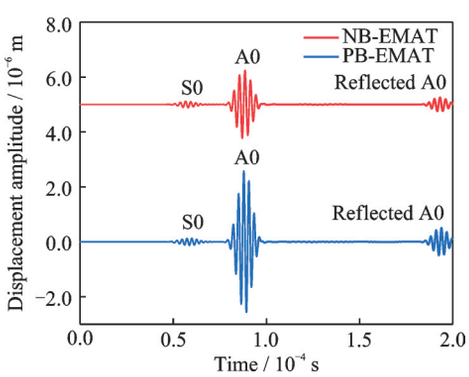

Fig.8 Displacements generated by NB-EMAT and PB-EMAT

3.2 Experimental analysis

To evaluate the influence of the bias magnetic field direction on MLC-EMATs, experimental analyses are conducted and are introduced in this section. The actual EMATs parameters are the same with the simulation model. Fig.9 shows the schematic diagram of the instrumentation set up for the experimental studies. To generate a strong current excitation signal, a RITEC RPR-4000 gated power amplifier is applied to the transmitter excitation coil. An arbitrary function generator is used to provide a modulated five-peak signal with a center frequency of 367 kHz. Between the power amplifier and the transmitter coil, an impedance matching network is configured. Two EMATs are placed on a 3 mm-thick aluminum plate as transmitter and receiver. The distance between the transmitter and the receiver is 500 mm.

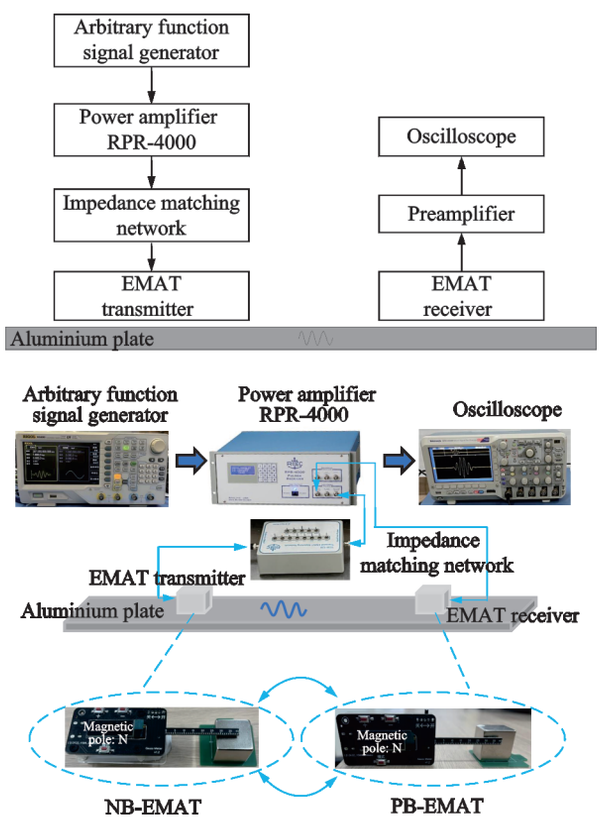

Fig.9 Schematic diagram of the experimental setup

To verify the conclusion obtained in previous section that the excitation efficiency of PB-EMAT for A0 mode Lamb waves is significantly stronger than NB-EMAT, four groups of experiments are conducted with different combinations of PB-EMAT and NB-EMAT as transmitters and receivers. It is worth stating that these two structures used

have the same setup except for the different magnetisation direction of the magnet. Fig.10 shows the signals tested with the four different experimental groups. For ease of comparison, we have placed them in one graph and appropriately raised the baseline of each signal. When the transmitter and receiver are both NB-EMATs, the tested signals are shown in Fig.10(a), marked as NB→NB. When the transmitter is NB-EMAT and the receiver is PB-EMAT, the tested signals are shown in Fig.10(b), marked as NB→PB. When the transmitter is PB-EMAT and the receiver is NB-EMAT, the tested signals are shown in Fig.10(c), marked as PB→NB. When the transmitter and receiver are both PB-EMATs, the tested signals are shown in Fig.10(d), marked as PB→PB. According to the reciprocity theorem, the amplitude of NB→PB and PB→NB should be the same, the tested signals shown in Fig.10(b) and Fig.10(c) are according with this conclusion, only with some minor errors which may be caused by the uneven magnetic field distribution of the magnet. The peak-to-peak amplitudes of tested signals in Fig.10(c) (PB→NB) and Fig.10(d) (PB→PB) are respectively 61% and 113% larger than that in Fig.10(a) (NB→NB). The comparison of these experimental results well proves that PB-EAMT can improve the excitation efficiency of A0 mode MLC-EMAT.

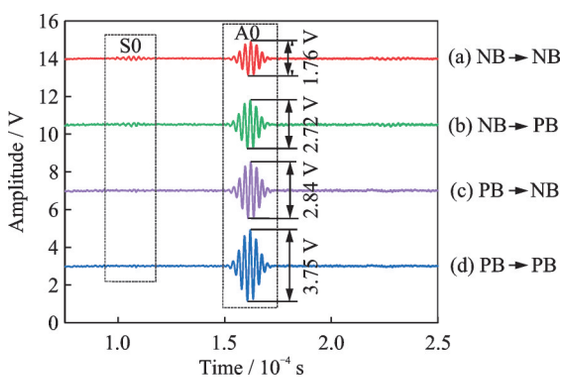

Fig.10 Different signals excited and received at 367 kHz

4 Conclusions

In this paper, the influence of bias magnetic field direction on the excitation efficiency of A0 mode Lamb waves in MLC-EMAT is investigated. The comparison of the magnetic field distribution of vertical and horizontal polarized magnets shows that the horizontal polarized magnet which has a dominated horizontal component of bias magnetic field can greatly increase the out-of-plane component of Lorentz force. Compared with traditional NB-EMAT, PB-EMAT is more suitable for exciting A0 mode Lamb waves whose displacements are mainly in the out-of-plane direction.

Further numerical and experiment results show that simply changing the magnets in the receiver or transmitter from vertical polarization to horizontal polarization, the excitation efficiency of the A0 mode can be increased by 61% (or 113% if the polarization directions of the magnets in both receiver and transmitter are changed from vertical to horizontal).

The results obtained in this paper can help us better understand the configuration rationality of the bias magnetic field in traditional MLC-EMAT, and offer a novel and convenient approach of using the bias magnetic field direction to improve the EMAT excitation efficiency. The method proposed here does not require complex design or optimization process as was introduced in Refs.[10, 12]. We also want to mention here that the optimizations of the magnet or coil structure are still important, and should be regarded as complementarity with the approach proposed in our work. The excitation efficiency of EMAT can be significantly improved by using our method in conjunction with other forms (magnet lift-off distance, magnet size, coil style, coil turns, etc.) of optimization in the next studies.

References

[1] THOMPSON R B. A model for the electromagnetic generation and detection of Rayleigh and Lamb waves[J]. IEEE Transactions on Sonics and Ultrasonics, 1973, 20: 340-346.

[2] THOMPSON R B. Mechanisms of electromagnetic generation and detection of ultrasonic Lamb waves in iron-nickel alloy polycrystals[J]. Journal of Applied Physics, 1977, 48: 4942-4950.

[3] THOMPSON R B. A model for the electromagnetic generation of ultrasonic guided wave in ferromagnetic metal polycrystals[J]. IEEE Transactions on Sonics

and Ultrasonics, 1978, 25: 7-15.
[4] VASILE C F, THOMPSON R B. Excitation of horizontally polarized shear elastic waves by electromagnetic transducers with periodic permanent magnets[J]. Journal of Applied Physics, 1979, 50: 2583-2588.
[5] KHALILI P, CAWLEY P. Relative ability of wedge-coupled piezoelectric and meander coil EMAT probes to generate single-mode lamb waves[J]. IEEE Transactions on Ultrasonics, Ferroelectrics, and Frequency Control, 2018, 65(4): 648-656.
[6] ZHANG W L, WU Y X, WU Y T, et al. An improved design of lamb wave EMAT for A0 wave generation and enhancement[J]. Japanese Journal of Applied Physics, 2021, 60(3): 036501.
[7] DU L R, GAO R Z, JIA X J. Antisymmetric Lamb wave simulation study based on electromagnetic acoustic transducer with periodic permanent magnets[J]. Sensors, 2023, 23(16): 7117.
[8] LIU J L, LIU S Z, ZHANG C, et al. A new focused EMAT design with narrow magnet to achieve both A0-Lamb signal enhancement and waveform distortion correction[J]. IEEE Sensors Journal, 2022, 22(15): 14786-14798.
[9] PENG S L, FAN Z B, WU Y X, et al. A type of focused single-mode A0 Lamb wave EMAT for performance improvement[J]. Japanese Journal of Applied Physics, 2025, 64(3): 036503.
[10] GUO X F, ZHU W J, QIU X L, et al. A Lorentz force EMAT design with racetrack coil and periodic permanent magnets for selective enhancement of ultrasonic Lamb wave generation[J]. Sensors, 2022, 23(1): 96.
[11] PEI C X, ZHAO S Q, XIAO P, et al. A modified meander-line-coil EMAT design for signal amplitude enhancement[J]. Sensors & Actuators: A. Physical, 2016, 247: 539-546.
[12] ZHANG J J, LIU M, JIA X J, et al. Numerical study and optimal design of the butterfly coil EMAT for signal amplitude enhancement[J]. Sensors, 2022, 22(13): 4985.
[13] LIU T H, PEI C X, CAI R, et al. A flexible and non-contact guided-wave transducer based on coils-only EMAT for pipe inspection[J]. Sensors & Actuators: A. Physical, 2020, 314: 112213.
[14] YANG X F, ZHANG W L, WU Y T, et al. An EMAT for improving the purity and amplitude of S0 Lamb waves[J]. Measurement Science and Technology, 2022, 33(9): 095114.
[15] LEE J K, KIM Y Y. Tuned double-coil EMATs for omnidirectional symmetric mode Lamb wave generation[J]. NDT & E International, 2016, 83: 38-47.
[16] LIU Z H, HU Y N, XIE M W, et al. Development of omnidirectional A0 mode EMAT employing a concentric permanent magnet pairs with opposite polarity for plate inspection[J]. NDT & E International, 2018, 94: 13-21.
[17] WILCOX P D. Modeling the excitation of Lamb and SH waves by point and line sources[C]//Proceedings of AIP Conference. Wisconsin, USA: Green Bay, 2003.
[18] WILCOX P D, LOWE M J S, CAWLEY P. The excitation and detection of Lamb waves with planar coil electromagnetic acoustic transducers[J]. IEEE Transactions on Ultrasonics, Ferroelectrics, and Frequency Control, 2005, 52(12): 2370-2383.

Acknowledgements This work was supported by the Foundation of Guangxi Key Laboratory of Manufacturing System and Advanced Manufacturing Technology (No.17-259-05-005Z) and Innovation Project of GUET Graduate Education (No.2025YCXS016).

Authors

The first author Mr. **LYU Zongmin** received his B.S. degree in engineering from Southwest Forestry University in 2022, and he is now pursing his M.S. degree at Guilin University of Electronic Technology. His main research interest focuses on electromagnetic ultrasonic detection technology.

The corresponding author Prof. **ZHANG Yinghong** received his Ph.D. degree in engineering from Nanjing University of Aeronautics and Astronautics in 2021. He is a senior experimentalist at School of Mechanical and Electrical Engineering, Guilin University of Electronic Technology, and a member of the Guangxi Key Laboratory of Manufacturing Systems and Advanced Manufacturing Technology. His research interests focus on advanced sensors, non-destructive testing technology, and mechanical analysis and testing.

Author contributions Mr. **LYU Zongmin** designed the study, complied the models, conducted the analysis, interpreted the results, and wrote the manuscript. Prof. **ZHANG Yinghong** contributed to data and model components for the EMAT model. Mr. **GUAN Wei** contributed to a preliminary validation of the study parameters and further proposed an optimisation scheme. Prof. **QIAN Zhenghua** contributed to the discussion and background of the study. All authors commented on the manuscript draft and approved the submission.

Competing interests The authors declare no competing interests.

(Production Editor: SUN Jing)

基于曲折线圈电磁超声换能器的A0波增强改进方法

吕宗民[1]，关 伟[2]，张应红[1]，钱征华[3]

（1.桂林电子科技大学机电工程学院，桂林 541004，中国；2.国营长虹机械厂，桂林 541004，中国；
3.南京航空航天大学航空学院，南京 210016，中国）

摘要：在传统的曲折线圈电磁超声换能器（Meander line coil electromagnetic acoustic transducer，MLC-EMAT）结构中，偏置磁场通常设置为沿板面法线方向。然而，由于反对称兰姆波的粒子振动始终由面外分量主导，采用垂直于板面的偏置磁场效率较低。本文研究了垂直偏置磁场电磁超声换能器（Normal bias magnetic field EMAT，NB-EMAT）与平行偏置磁场电磁超声换能器（Parallel bias magnetic field EMAT，PB-EMAT）在发射和接收A0模态兰姆波时的性能表现，并详细阐述了这两种结构的工作机制。首先建立了两种结构的有限元模型，通过数值计算求解其磁场分布，并将结果与实验数据进行对比验证。然后，通过对比两个电磁超声换能器激发的洛伦兹力分布，证明了通过选择偏置磁场方向可有效提升MLC-EMAT的激励效率。此外，在仿真软件中对NB-EMAT与PB-EMAT的激励效率进行了定量分析与对比，结果表明PB-EMAT的激励效率比NB-EMAT高出108%。最后，多组对比实验验证了数值计算所得结论。实验结果表明：仅需将传统NB-EMAT替换为PB-EMAT，激励效率即可提升50%以上；若同时采用PB-EMAT作为收发器，激励效率可进一步提升113%。

关键词：电磁超声换能器；曲折线圈；兰姆波；A0波；平行偏置磁场